◆IEEE

Optimal PI Based Secondary Control for Autonomous Micro-grid via Particle Swarm Optimization Technique

M. A. Ebrahim
Electrical Engineering Department,
Faculty of Engineering at Shoubra, Benha University,
Cairo, Egypt
mohamed.mohamed@feng.bu.edu.eg;

Beshoy Abdou Aziz, F. A. Osman
Electrical Engineering Department,
Benha Faculty of Engineering, Benha University,
Qalubia, Egypt
eng.beshoyabdou@yahoo.com;

Maged N. F. Nashed
Power Electronics and Energy Conversion Department,
Electronics Research Institute,
Cairo, Egypt
maged@eri.sci.eg;

Abstract—**Hybrid micro-grids require harmony operation of renewable energy resources based voltage source inverters (VSIs) in grid-tied as well as islanded modes. In this paper, the modeling, analysis, and control strategy of VSIs based autonomous micro-grid are developed. An integrated control system for autonomous micro-grid is carried out including two control levels. The primary control level is comprised of the current and voltage inner control loops, the virtual inductor loops, and the droop control loops. This control level is necessary to regulate voltage and frequency, and also to achieve accurate power sharing among the paralleled distributed generators (DGs). However, the secondary control level is employed to eliminate the voltage magnitude and angular frequency deviations produced by primary control level. The parameters of secondary controllers are optimized using particle swarm optimization technique to achieve good dynamic and steady state performance for micro-grid voltage and frequency. Two micro-grid structures are modeled and simulated in MATLAB environment to accomplish this study. The first structure consists of only one distributed generation unit, while the second contains four DGs. Each structure is tested with and without secondary control level under the load variations to confirm the robustness of the control system. The results of the traditional and optimized secondary controllers are compared.**

Keywords— autonomous micro-grids, distributed generation, particle swarm optimization, secondary control

I. INTRODUCTION

Nowadays, the growth of micro-grids is rapidly increasing. A micro-grid consists of distributed generation (DG) sources based on renewable energy connected beside the loads to facilitate the distribution of power systems [1]. Fig.1 represents the basic structure of micro-grids. Power sharing is the major concern when various DGs work in parallel operation. It is necessary to obtain a proper power sharing when multiple DGs are paralleled to operate together. One of the most common methods for power sharing is the droop control method [2, 3]. It needs only to the local measurements for feedback signals (voltages and currents). This technique is employed to obtain good power sharing among independent DGs through low-bandwidth data communication signals between each generator [4].

Micro-grids can work in grid-tied mode and autonomous (islanded) mode [5]. One of the widely used control strategies for micro-grids is the hierarchical control strategy including primary, secondary, and tertiary control levels [6].

Due to the advantages of droop control strategy mentioned above, the primary control level depends on it, in order to achieve accurate load sharing. Moreover, the voltage and frequency of micro-grid are regulated for both operating modes by primary control. The secondary control is used to eliminate any deviations in frequency and voltage magnitude produced by droop control [7]. Furthermore, the micro-grid re-synchronization with the utility grid can be achieved by secondary control. The tertiary level is responsible for controlling the power flow among the DGs and utility grid to optimize the micro-grid operational cost. It is mostly incorporated when the micro-grid is in grid-tied operation. Furthermore, the tertiary level is sometimes used in autonomous operation for economic considerations. This paper focuses on the autonomous micro-grid including only primary and secondary control levels. Moreover, the proportional-integral coefficients of secondary controllers are determined using particle swarm optimization (PSO) technique to enhance the dynamic and steady-state behavior of micro-grid voltage and frequency.
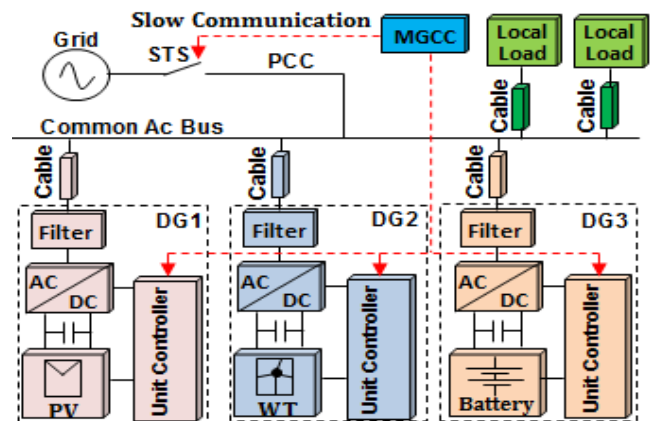

Fig. 1. Basic structure of micro-grids (MGCC: Micro-Grid Central Control /PV: Photovoltaic /WT: Wind Turbine /PCC: Point of Common Coupling).

The structure of this paper is as follows: In Section II, the modeling and control strategy of DG unit are represented. Section III shows the frequency response and stability analysis for DG unit. Section IV explains the droop control strategy. Section V introduces the secondary control strategy. Section VI presents PSO technique used for optimizing the coefficients of secondary controllers. Section VII illustrates the simulation results. Finally, Section VIII introduces the conclusion of this article.

1148

II. ANALYSIS AND CONTROL STRATEGY FOR THREE-PHASE VSI

Fig. 2 displays the power circuit of the VSI for DG unit comprising a three-phase PWM inverter and an LC filter plus coupling impedance. Neglecting the connected loads and the coupling impedance, the analysis and modeling of VSI in synchronous $d - q$ frame can be represented as:

$$\begin{cases} Lf \frac{di_{Lfd}}{dt} = V_{id} - V_{cd} - R_f i_{Lfd} + \omega L_f i_{Lfq} \\ Lf \frac{di_{Lfq}}{dt} = V_{iq} - V_{cq} - R_f i_{Lfq} - \omega L_f i_{Lfd} \end{cases} \quad (1)$$

$$\begin{cases} Cf \frac{dV_{cd}}{dt} = i_{Lfd} - i_{od} + \omega C_f V_{cq} \\ Cf \frac{dV_{cq}}{dt} = i_{Lfq} - i_{oq} - \omega C_f V_{cd} \end{cases} \quad (2)$$

where ω is the angular frequency of the micro-grid, i_{Lfd}, i_{Lfq}, V_{id} and V_{iq} are the currents through filter inductor and inverter side voltages in $d - q$ frame, respectively, and V_{cd}, V_{cq}, i_{od} and i_{oq} are the filter capacitor voltages and output currents in $d - q$ frame.
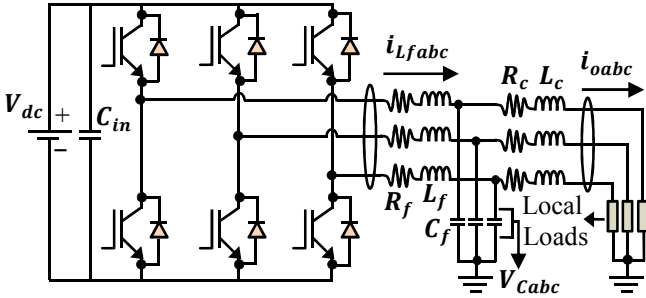
Equations (1) and (2) clarify that the derivative of both d-axis and q-axis currents, i_{Lfd} and i_{Lfq}, are related to both d and q axis variables. Furthermore, the derivative of both d-axis and q-axis voltages, V_{cd} and V_{cq}, are related to both d and q axis variables. This indicates that the system control is cross-coupled, which may cause problems in controller design and poor dynamic performance. To solve this concern, the decoupled terms can be added as shown in Fig. 3. The output of the decoupled controllers shown in Fig. 3 can be expressed as:

$$\begin{cases} i_{dref} = G_v(s)\left(V_{dref} - V_{cd}\right) - \omega C_f V_{cq} \\ i_{qref} = G_v(s)\left(V_{qref} - V_{cq}\right) + \omega C_f V_{cd} \\ V_{id} = V_{dpwm} = G_i(s)\left(i_{dref} - i_{Lfd}\right) + V_{cd} - \omega L_f i_{Lfq} \\ V_{iq} = V_{qpwm} = G_i(s)\left(i_{qref} - i_{Lfq}\right) + V_{cq} + \omega L_f i_{Lfd} \end{cases} \quad (3)$$

Here, V_{dref}, V_{qref}, i_{dref} and i_{qref} are the reference values of voltage and current loops in $d - q$ frame, while $G_v(s)$ and $G_i(s)$ are the controllers for the $d - q$ axis voltages and currents, respectively. In this paper, these controllers are of the proportional-integral type.

The primary control strategy for DG unit, shown in Fig. 3, includes six feedback control loops: four inner voltage and current loops for a proper control of $d - q$ axis voltages and currents V_{cd}, V_{cq}, i_{Lfd} and i_{Lfq}, respectively, and two outer feedback loops for controlling the real and reactive power. The outer loops are called droop control loops needed for achieving power sharing among DG units connected in parallel. Moreover, there are two intermediate control loops named virtual output impedance loops, which can be employed to adapt the output impedances of VSIs [8]. Both the outer and virtual inductor loops will be discussed in the next sections.
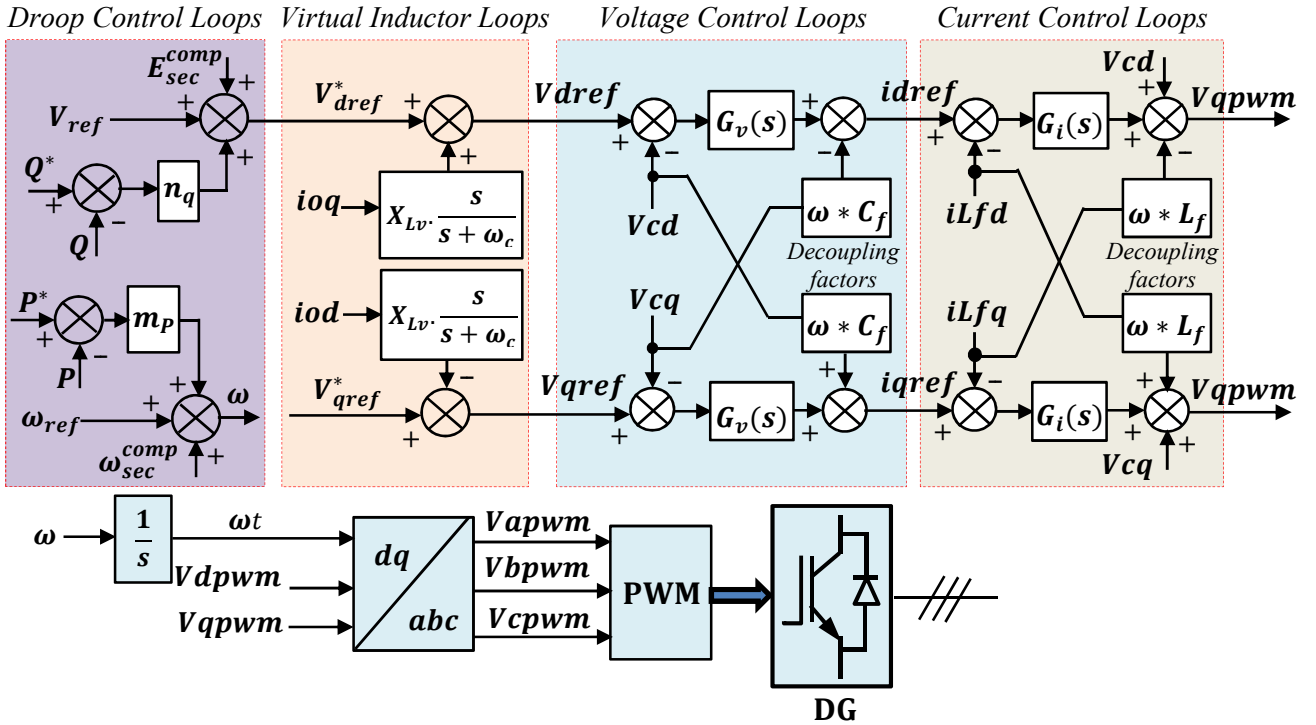

Fig. 2. Power circuit of the VSI for DG unit operated in islanded mode.

Fig. 3. Primary control strategy for distributed generation unit.

III. FREQUENCY RESPONSE AND STABILITY ANALYSIS FOR VSI

The closed loop dynamics of the VSI, shown in Fig. 4, can be analyzed using Mason's theorem for block diagram reduction purposes. The output voltage can be derived from Fig. 4 as the following:

$$V_{cf}(s) = G(s)V_{ref}(s) - Z_o(s)I_o(s) \qquad (4)$$

where

$$G(s) = \frac{G_v(s)G_i(s)G_{PWM}(s)}{L_f C_f s^2 + \left(C_f s + G_v(s)\right)G_i(s)G_{PWM}(s) + C_f R_f s + 1} \qquad (5)$$

$$Z_o(s) = \frac{L_f s + R_f + G_i(s)G_{PWM}(s)}{L_f C_f s^2 + \left(C_f s + G_v(s)\right)G_i(s)G_{PWM}(s) + C_f R_f s + 1} + \\ G(s)Z_v(s) \qquad (6)$$

$$G_{PWM}(s) = \frac{1}{1 + \frac{3}{2}T_s s} \qquad (7)$$

$$G_v(s) = K_{pv} + \frac{Kiv}{s} \qquad (8)$$

$$G_i(s) = K_{pi} + \frac{Kii}{s} \qquad (9)$$

Here, $G(s)$ is the closed loop transfer function that shows the relationship between V_{cf} and V_{ref}, T_s is the sampling time, $Z_o(s)$ is the closed loop output impedance, K_{iv} and K_{pv} are the integral and proportional coefficients for voltage controller, respectively, K_{ii} and K_{pi} are the integral and proportional coefficients for current controller, respectively, and $Z_v(s)$ is the virtual impedance, which can be expressed as:

$$Z_v(s) = s.L_v \qquad (10)$$

where L_v is the virtual impedance inductance. The virtual inductor loops are needed to increase the inductivity of the inverter output impedance to prevent the cross-coupling between real and reactive powers. Therefore, the real power is proportional to the power angle, while the reactive power is proportional to the voltage. However, the increasing of virtual inductor may lead the transient performance to deteriorate. Therefore, the high-pass filter is employed with the virtual inductor, as in [9]. Moreover, the virtual inductor is necessary for parallel operation of VSIs [10, 11], and can be implemented by additional physical inductors, but the size and cost will be increased [12].
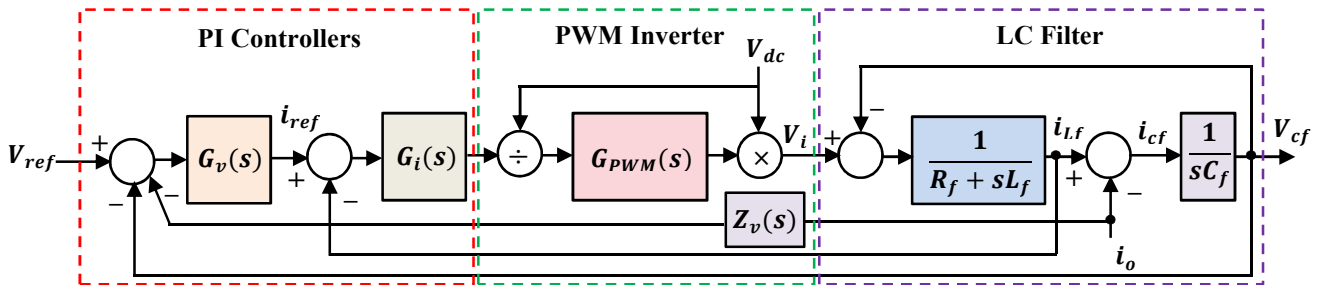
Fig. 5 shows the closed loop bode plot of output voltages for both DG1 and DG2. The gain margins for DG1 and DG2 are 30.5 dB at angular frequency of 28100 rad/s and 19.1 dB at angular frequency of 10200 rad/s, and phase margins are 83.2º at angular frequency of 4260 rad/s and 91.9º at angular frequency of 3250 rad/s, respectively. The parameters of the DG units are listed in Table I.
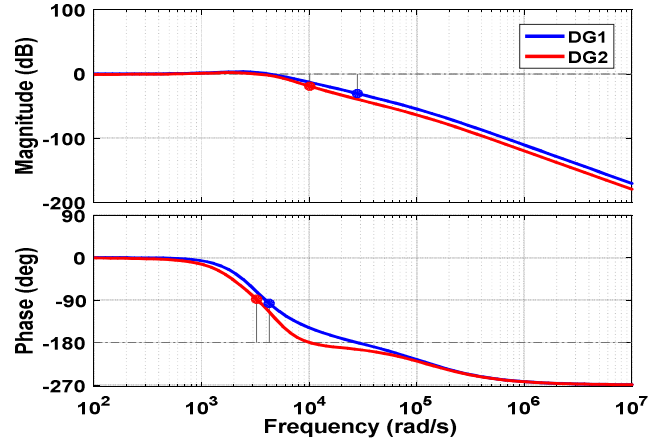

Fig. 5. Closed loop bode plot of the output voltages for DG1 and DG2.

Fig. 6 illustrates the frequency response of closed loop output impedances for DG1 and DG2 without and with virtual inductor of 2 mH. As can be observed, the output impedances of DG1 and DG2 have a highly inductive behavior in the area below the natural angular frequency that is necessary to accurate operation of droop control operation.
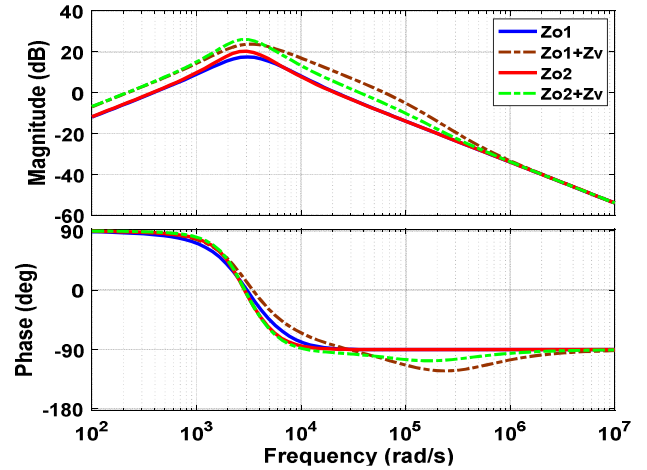

Fig. 6. Closed loop bode plot of the output impedances for DG1 and DG2 without and with virtual inductor of 2 mH.

Fig. 4. Closed loop system block diagram of VSI with virtual impedance.

IV. DROOP CONTROL STRATEGY FOR POWER SHARING AMONG PARALLELED VSIs

The droop control technique has been proposed for islanded micro-grids to obtain a proper power sharing between paralleled DGs with only low-bandwidth communications. There are many types of droop control depend on the type of DG output impedance, whether it is pure inductor, resistor, capacitor, or other types [13]. In this paper, the inductive type only is discussed because the network is assumed to have high X/R ratio. The equivalent circuit diagram of the VSI connected to a micro-grid bus $(V_2 \angle 0)$, displayed in Fig. 7, is used to explain and simplify the principle of the droop techniques. The model of the VSI can be represented by AC voltage source, $V_1 \angle \delta$, with series output impedance, $Z_o \angle \theta_o$, as shown in (4).
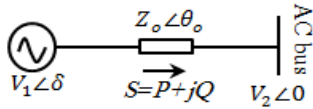

Fig. 7. Equivalent circuit of a VSI connected to the micro-gird.

The apparent power of a VSI supplied to the micro-grid bus can be expressed as:

$$S = V_2 I^* = \frac{V_1 V_2 \angle \theta_o - \delta}{Z_o} - \frac{V_2^2 \angle \theta_o}{Z_o} \qquad (11)$$

$$\begin{cases} P = \frac{V_1 V_2}{Z_o} \cos(\theta_o - \delta) - \frac{V_2^2}{Z_o} \cos \theta_o \\ Q = \frac{V_1 V_2}{Z_o} \sin(\theta_o - \delta) - \frac{V_2^2}{Z_o} \sin \theta_o \end{cases} \qquad (12)$$

In this paper, the output impedance of VSIs, $Z_o \angle \theta_o$, is tended to be more inductive ($\theta_o \cong 90°$), as shown in Fig. 6, consequently (12) is reduced to

$$\begin{cases} P = \frac{V_1 V_2}{Z_o} \sin \delta \\ Q = \frac{V_1 V_2 \cos \delta - V_2^2}{Z_o} \end{cases} \qquad (13)$$

If the power angle, δ, has very small value, then, $\sin \delta \cong \delta$ and $\cos \delta \cong 1$.

$$\begin{cases} P \cong \frac{V_1 V_2}{Z_o} \delta \\ Q \cong \frac{V_1 V_2 - V_2^2}{Z_o} \end{cases} \qquad (14)$$

and, approximately

$$P \propto \delta \quad , \quad Q \propto V_1 \qquad (15)$$

Thus, the droop control method for the inductive output impedance can be formed in the following equation:

$$\begin{cases} V_i = V^* - n_{qi} Q_i \\ \omega_i = \omega^* - m_{pi} P_i \end{cases} \qquad (16)$$

where V^* is the peak value of the VSI output voltage at no load condition, ω^* is the no load angular frequency, and n_{pi}

and m_{qi} are the droop coefficients for reactive and real power, respectively. In order to obtain a proper power sharing between the paralleled independent DGs, the following constraints must be satisfied:

$$\begin{cases} m_{p1} P_1 = m_{p2} P_2 = \cdots = m_{pi} P_i = \Delta\omega_{max} \\ n_{q1} Q_1 = n_{q2} Q_2 = \cdots = n_{qi} Q_i = \Delta V_{max} \end{cases} \qquad (17)$$

where ΔV_{max} and $\Delta\omega_{max}$ are the permissible limits for voltage magnitude and angular frequency deviations, respectively.

V. SECONDARY CONTROL FOR COMPENSATING ANY DEVIATIONS IN VOLTAGE AND FREQUENCY

The main function of secondary control is to eliminate any deviations in voltage amplitude and angular frequency produced by the primary control. The correction of these deviations must be within limits accepted by grid code requirements. Fig. 8 displays the main structure of secondary control. The compensation parts needed to restore the desired values of angular frequency and voltage magnitude are derived as [14, 15]:

$$\omega_{sec}^{comp} = K_{p\omega}\left(\omega_{MG}^{ref} - \omega_{MG}^{meas}\right) + K_{i\omega} \int\left(\omega_{MG}^{ref} - \omega_{MG}^{meas}\right)dt \qquad (18)$$

$$E_{sec}^{comp} = K_{pE}\left(E_{MG}^{ref} - E_{MG}^{meas}\right) + K_{iE} \int\left(E_{MG}^{ref} - E_{MG}^{meas}\right)dt \qquad (19)$$

where ω_{MG}^{ref} and ω_{MG}^{meas} are the reference and measured values of micro-grid angular frequency, and E_{MG}^{ref} and E_{MG}^{meas} are the reference and measured values of micro-grid voltage amplitude, respectively, while $K_{p\omega}$, $K_{i\omega}$, K_{PE}, and k_{iE} are the PI coefficients of secondary controllers. In this paper, these coefficients are tuned by both the traditional method and PSO technique.
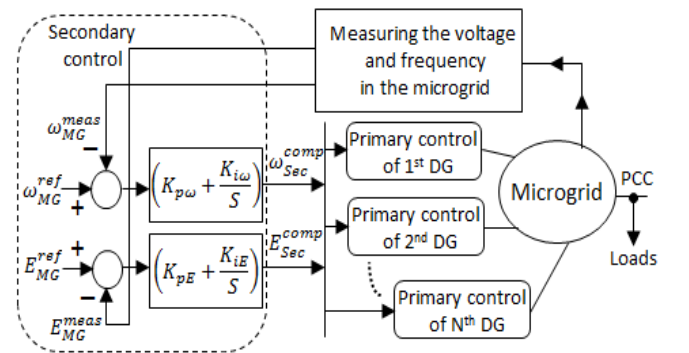

Fig. 8. The main structure of secondary control.

VI. PATICLE SWARM OPTIMIZATION TECHNIQUE

The PSO technique has been suggested as a metaheuristic algorithm since 23 years ago. The main steps and flow chart of this algorithm are described in [16]. PSO has been recently used in many engineering problems, especially in a micro-grid control system to adjust the droop coefficients, as in [17]. In this paper, the PSO algorithm is employed for a proper selection of secondary controller parameters. The objective function has been selected to minimize the integration of time multiplied by the squared error of voltage amplitude and angular frequency.

VII. SIMULATION AND RESULTS

Two autonomous micro-grid systems are modeled and simulated using MATLAB environment. The first system is discussed in case (1) for a micro-grid containing only one DG unit, as displayed in Fig. 9. The second system is explained in case (2) for a micro-grid consisting of four DGs, as shown in Fig. 15. In two cases, the micro-grid is tested with and without secondary control under the load variations. The performance of traditional and optimized controllers for secondary level is evaluated and compared under the load variations to confirm the robustness of the proposed secondary controllers.

A. Case (1)
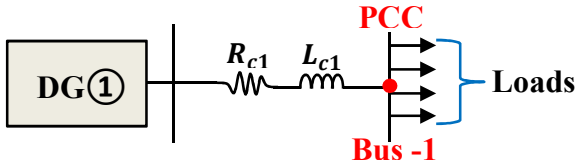
Fig.9. Structure of tested micro-grid for case (1).

Fig. 10 depicts the variations of load connected to micro-grid system shown in Fig (9). The frequency and voltage magnitude under load variations are shown in Figures 11 and 12, respectively. It can be observed that without secondary control, there are many deviations from the set-points of frequency and voltage magnitude. These deviations depend on the loads connected at the point of common coupling (PCC) of the micro-grid. The frequency and voltage magnitude are restored to set-points (i.e. 50 Hz and 311.13 V) by using the secondary control. In the case of the optimized secondary controller, the transient oscillations in voltage magnitude and frequency are highly damped compared to the traditional controller. Moreover, the steady-state time is reduced for the voltage and frequency response compared to the traditional controller. Figures 13 and 14 illustrate the output real and reactive powers of the distributed generator displayed in Fig. 9. These real and reactive powers are measured at PCC without and with secondary control under the load variations. In the case of applying the secondary control, the output real and reactive powers are significantly high compared to the case of without secondary control. However, the responses of real and reactive powers for both traditional and optimized secondary controllers are almost the same.
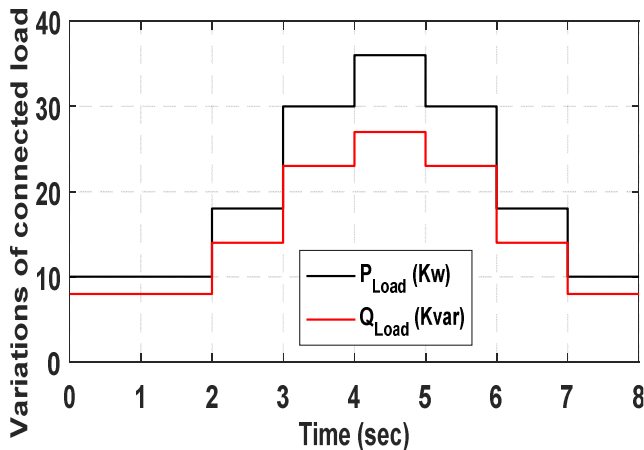
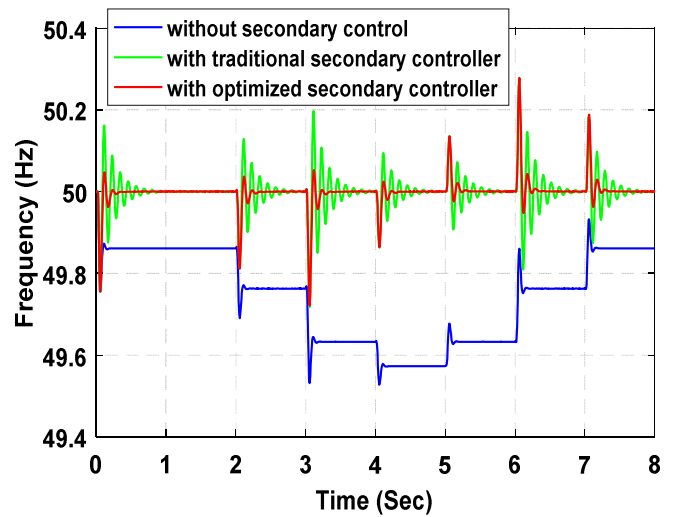

Fig.10. Variations of connected load for case (1).

Fig.11. Frequency at PCC of tested micro-grid without and with secondary control under load variations.
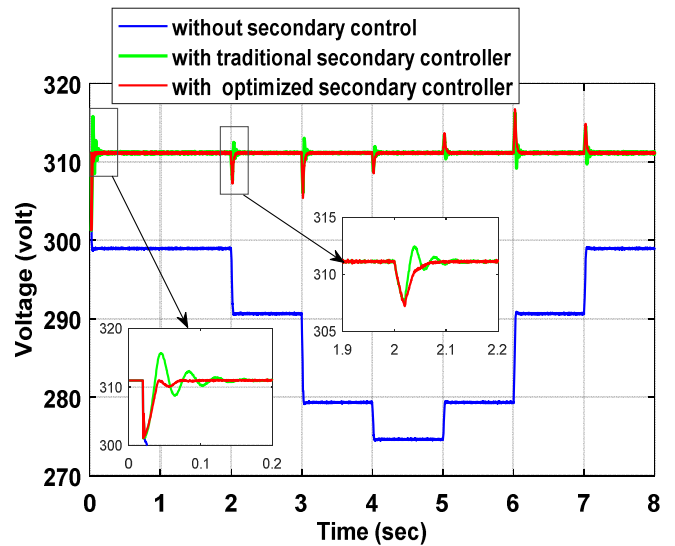

Fig.12. Voltage magnitude at PCC of tested micro-grid without and with secondary control under load variations.
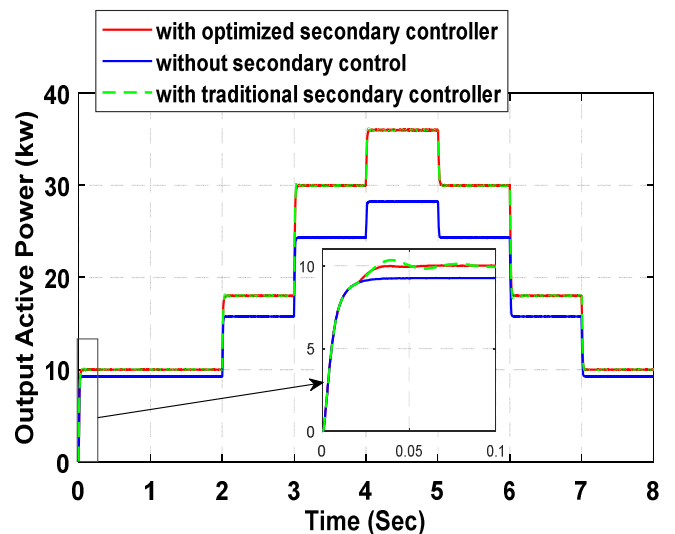

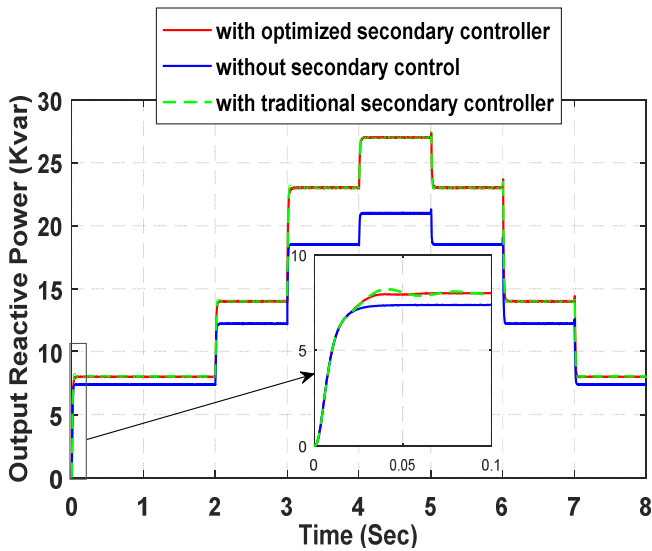Fig.13. Real power at PCC of tested micro-grid without and with secondary control under load variations.

Fig.14. Reactive power at PCC of tested micro-grid without and with secondary contro under load variations.
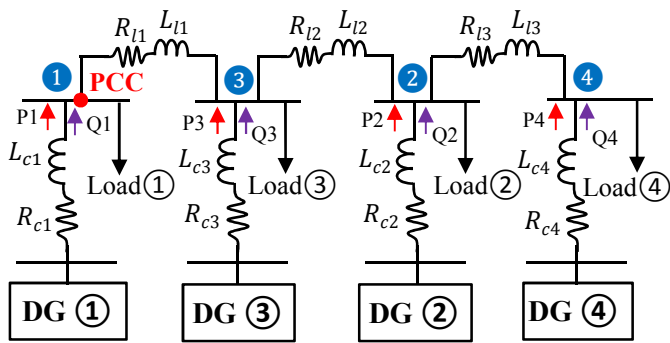
B. Case (2)

Fig.15. Structure of tested microgrid for case (2).

Fig. 16 shows the powers of the loads connected to the micro-grid displayed in Fig. 15. This micro-grid consists of four DG units and four local loads. Fig. 17 illustrates the frequencies of DG units with and without activating the traditional secondary control under the load variation. It can be observed that the frequencies of DG units are increased from 49.78 Hz to 50 Hz by activating the traditional secondary control at the time of 1 sec. This value (50 Hz) remains constant under the load variation at the time of 3 sec. However, there are many transient oscillations, which can be significantly damped by optimizing the secondary controllers as shown in Fig. 20. Moreover, the steady-state time of frequencies response is reduced by using the optimized secondary controllers.

The voltages magnitudes of DG units with and without activating the traditional secondary control under the load variation are depicted in Fig. 18. It can be observed that the voltage magnitude is increased from 298.8 V to 311.2 V for DG1, from 294.6 V to 306.8 V for DG2, from 297.3 V to 309.6 V for DG3, and from 295.8 V to 308 V for DG4, that by activating the traditional secondary control at the time of 1 sec. Furthermore, the voltage magnitude under the load variation at the time of 3 sec is remained constant at 311.2 V for DG1, increased from 306.8 V to 309.5 V for

DG2, increased from 309.6 V to 311.2 V for DG3, and increased from 308 V to 310 V for DG4. The transient oscillations caused by the traditional controllers can be minimized by using the optimized secondary controllers, as illustrated in Fig. 21. Moreover, the steady-state time for the responses of voltages is reduced.

Fig. 19 shows the output real powers for DG units with and without activating the traditional secondary control under the load variation. It can be observed that the real output power is increased from 14.9 KW to 16.1 KW for both DG1 and DG3, and from 11.2 KW to 12.2 KW for both DG2 and DG4. Moreover, this output power under the load variation at the time of 3 sec is increased from 16.1 KW to 18.3 KW for both DG1 and DG3, and from 12.2 KW to 13.7 KW for both DG2 and DG4. Fig. 22 has almost the same characteristics as Fig. 19.

Fig. 23 represents the real power sharing among DG units under the load variation with and without activating the optimized secondary control. It can be observed that each DG unit shares with the same percentage value of its rated power as other units, that as the desired settings. The real power sharing of each DG unit is increased from 41.2% to 45.9% by activating the secondary control at the time of 1 sec. Then, it is increased from 45.9% to 50.8% by increasing the load at the time of 3 sec.

Thanks to the droop control, a proper power sharing among the independent paralleled DGs has been achieved. Moreover, the desired values of frequency and voltage magnitude have been restored without any deviations under load variation, that by activating the secondary control. Additionally, an accurate selection of secondary controller parameters has been obtained using PSO technique. Finally, it can be concluded that the responses of voltages and frequencies for all DGs are improved by using the optimized secondary controllers.
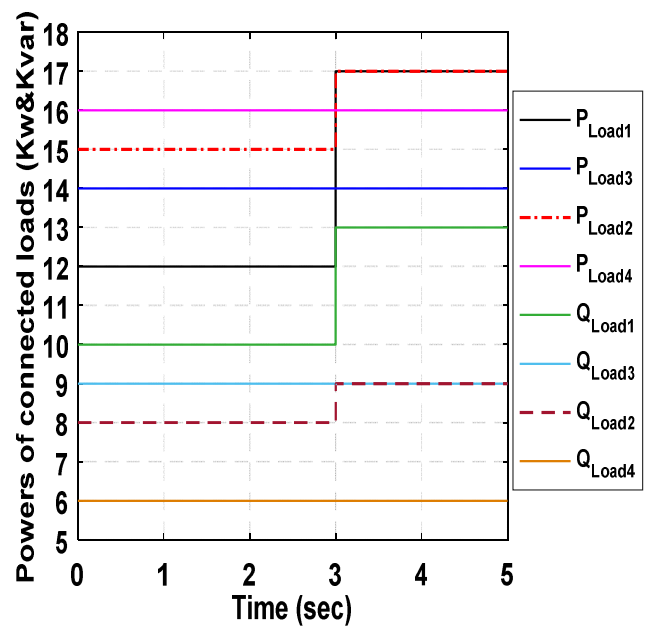

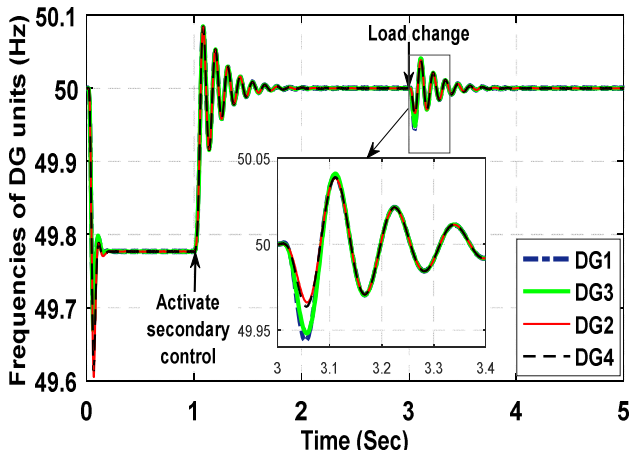Fig.16. Powers of connected loads for case (2).

Fig.17. Frequencies of DG units without and with activating traditional secondary control under load variation.
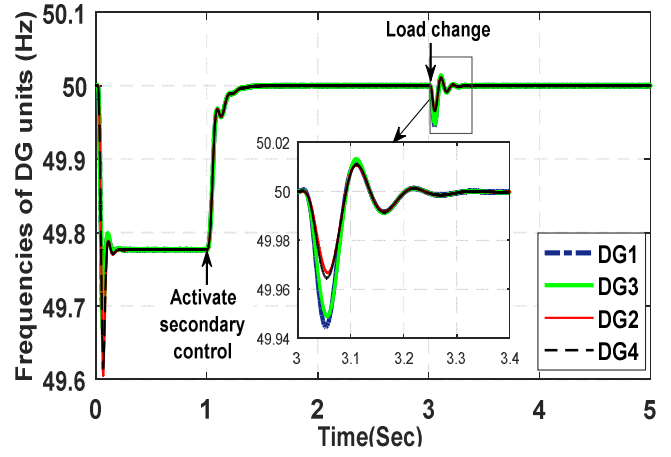

Fig.20. Frequencies of DG units without and with activating optimized secondary control under load variation.
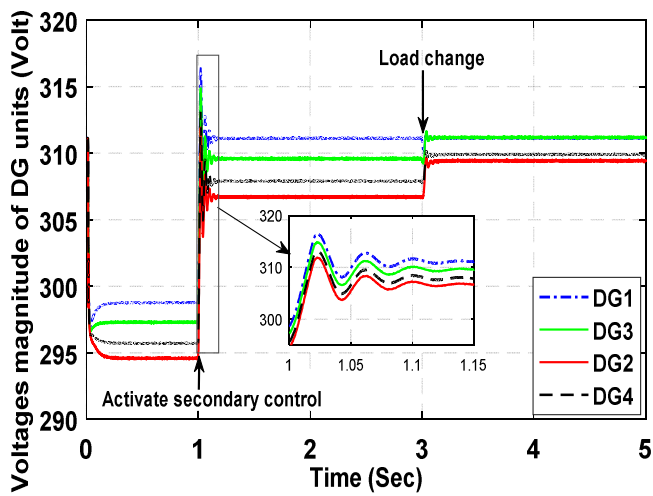

Fig.18. Voltages magnitudes of DG units without and with activating traditional secondary control under load variation.
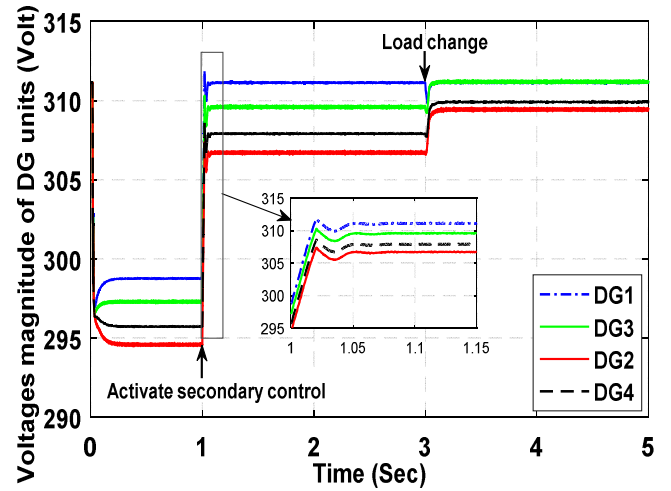

Fig.21. Voltages magnitudes of DG units without and with activating optimized secondary control under load variation.
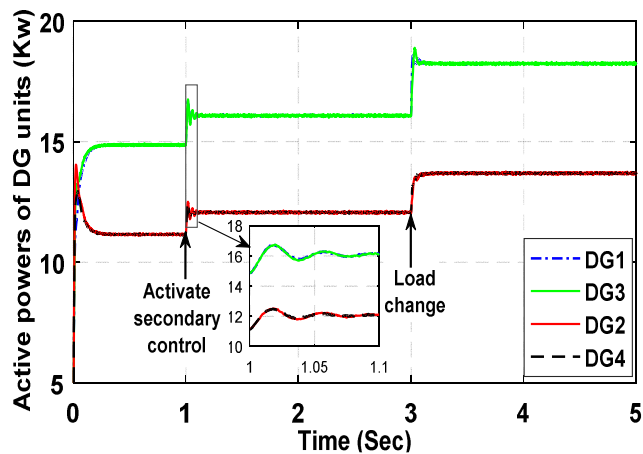

Fig.19. Real powers of DG units without and with activating the traditional secondary control under load variation.
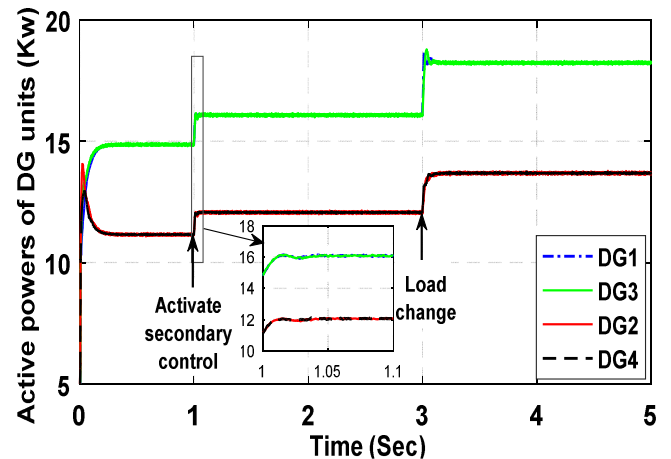

Fig.22. Real powers of DG units without and with activating optimized secondary control under load variation.
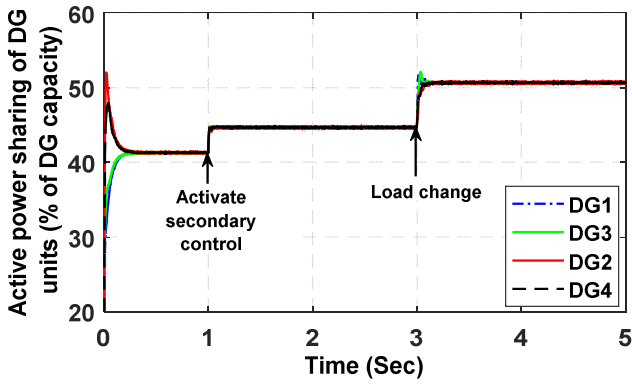
Fig.23. Real power sharing of DG units (% of DG rated active power) without and with secondary control under load variation.

TABLE I.   PARAMETERS OF TESTED MICRO-GRID.

DGs	DG1 & DG3		DG2 & DG4	
	$P1_{rated}$	36 KW	$P2_{rated}$	27 KW
	$Q1_{rated}$	27 KVAR	$Q2_{rated}$	20 KVAR
	m_{p1}	9.4×10^{-5}	$mp2$	12.533×10^{-5}
	$nq1$	1.3×10^{-3}	$nq2$	1.755×10^{-3}
	$Rc1$	30 m Ω	$Rc2$	30 m Ω
	$Lc1$	0.35 mH	$Lc2$	0.35 mH
	$Rf1$	100 m Ω	$Rf2$	100 m Ω
	$Lf1$	1350 μH	$Lf2$	1350 μH
	$Cf1$	0.05 mF	$Cf2$	0.05 mF
	$XLv1$	600 m Ω	$XLv2$	600 m Ω
	$Vdc1$	750 V	$Vdc2$	750 V
	$Vref1$	311.13 V (Peak)	$Vref2$	311.13 V (Peak)
	$Fref1$	50 Hz	$Fref2$	50 Hz
	Ts	5×10^{-6} Sec.	Ts	5×10^{-6} Sec.
Transmission Lines	T.L1		T.L2	T.L3
	RL1	230 m Ω	RL2 350 m Ω	RL3 230 m Ω
	Ll1	0.318 mH	Ll2 1.847 mH	Ll3 0.318 mH

VIII. CONCLUSION

In this paper, the modeling, analysis, and control strategy have been performed for VSIs based autonomous microgrid. Two levels of control have been applied to the microgrid test system. The primary control level has been utilized for frequency and voltage regulation in addition to achieving accurate power sharing between paralleled DG units. While, the secondary control level has been applied and optimized using PSO technique to compensate any deviations in frequency and voltage caused by primary level. Tests have been done on both a microgrid including only one DG unit and a microgrid consisting of four DG units. The optimized secondary controller gives good performance for both dynamics and steady state.

REFERENCES

[1] Khamis, A., Mohamed, A., Shareef, H., Ayob, A. and Saharuddin, N.Z., "Methodologies of a microgrid testbed using renewable energy based power generation", In Computer Modeling and Simulation (EMS), 2012 Sixth UKSim/AMSS European Symposium on IEEE, pp. 132-136, November 2012.

[2] Wu, D., Tang, F., Dragicevic, T., Vasquez, J.C. and Guerrero, J.M., "A control architecture to coordinate renewable energy sources and energy storage systems in islanded microgrids," IEEE Transactions on Smart Grid, vol. 6, no. 3, pp. 1156–1166, May 2015.

[3] Guerrero, J.M., Chandorkar, M., Lee, T.L. and Loh, P.C.,, "Advanced control architectures for intelligent microgrids-part i: Decentralized and hierarchical control," IEEE Transactions on Industrial Electronics vol. 60, no. 4, pp. 1254–1262, April 2013.

[4] Guerrero, J.M., De Vicuna, L.G., Matas, J., Castilla, M. and Miret, J., "A wireless controller to enhance dynamic performance of parallel inverters in distributed generation systems", IEEE Transactions on power electronics", vol. 19, no. 5, pp.1205-1213, September 2004.

[5] Kroposki, B., Lasseter, R., Ise, T., Morozumi, S., Papatlianassiou, S. and Hatziargyriou, N., "Making microgrids work," IEEE Power and Energy Magazine, vol. 6, pp. 40-53, 2008.

[6] Bidram, A. and Davoudi, A., "Hierarchical structure of microgrids control system," IEEE Transactions on Smart Grid, vol. 3, no. 4, pp.1963-1976, 2012.

[7] Mahmoud, M.S. and Hussain, S.A., "Adaptive PI secondary control for smart autonomous microgrid systems," International Journal of Adaptive Control and Signal Processing, vol. 29, no. 11, pp.1442-1458, November 2015.

[8] Yao, W., Chen, M., Matas, J., Guerrero, J.M. and Qian, Z.M., "Design and analysis of the droop control method for parallel inverters considering the impact of the complex impedance on the power sharing," IEEE Transactions on Industrial Electronics, vol. 58, no. 2, pp. 576-588, February 2011.

[9] Guo, Z., Sha, D. and Liao, X., "Voltage magnitude and frequency control of three-phase voltage source inverter for seamless transfer," IET Power Electronics, vol. 7, no. 1, pp. 200-208, January 2014.

[10] Guerrero, J., Matas, J., Vicuna, L., Castilla, M., Miret, J., "Decentralized control for parallel operation of distributed generation inverters using resistive output impedance," IEEE Trans. Ind. Electron., vol. 54, no. 2, pp. 994–1004, 2007.

[11] Guerrero, J.M., Matas, J., de Vicuna, L.G., Castilla, M., Miret, J., "Wireless-control strategy for parallel operation of distributed-generation inverters," IEEE Trans. Ind. Electron., vol. 53, no. 5, pp. 1461–1470, 2006.

[12] Issa, W.R., Abusara, A. and Sharkh, S.M., "Impedance interaction between islanded parallel voltage source inverters and the distribution network," 7th IET International Conference on Power Electronics, Machines and Drives (PEMD 2014), April 2014.

[13] Zhong, Q.C., "Harmonic droop controller to reduce the voltage harmonics of inverters," IEEE Transactions on Industrial Electronics, vol. 60, no. 3, pp. 936-945, March 2013.

[14] Vasquez, J.C., Guerrero, J.M., Savaghebi, M., Eloy-Garcia, J. and Teodorescu, R., "Modeling, analysis, and design of stationary-reference-frame droop-controlled parallel three-phase voltage source inverters,"IEEE Transactions on Industrial Electronics, vol. 60, no. 4, pp. 1271-1280, April 2013.

[15] Bidram, A., Nasirian, V., Davoudi, A. and Lewis, F.L., "Cooperative Synchronization in Distributed Microgrid Control," Springer, February 2017.

[16] Polprasert, J., Ongsakul, W. and Dieu, V.N., "Optimal reactive power dispatch using improved pseudo-gradient search particle swarm optimization," Electric Power Components System, Vol. 44, pp. 518-532, 2016.

[17] Chung, I.Y., Liu, W., Cartes, D.A. and Schoder, K., "Control parameter optimization for a microgrid system using particle swarm optimization," in Proc. IEEE Int. Conf. Sustainable Energy Technologies, pp. 837–842, 2008.